Engineering Structures 236 (2021) 112040

Contents lists available at ScienceDirect

Engineering Structures

journal homepage: www.elsevier.com/locate/engstruct

Experimental investigation on flexural behaviour of vertically-curved circular-hollow steel sections strengthened with externally bonded carbon fibre reinforced polymer

K.A.B. Weerasinghe [a,*], J.C.P.H. Gamage [b], Sabrina Fawzia [c], D.P. Thambiratnam [c]

[a] Institute of Technology, University of Moratuwa, Sri Lanka
[b] Department of Civil Engineering, University of Moratuwa, Sri Lanka
[c] School of Civil & Environmental Engineering, Faculty of Science and Engineering, Queensland University of Technology, Brisbane, Queensland, Australia

ARTICLE INFO

Keywords:
Steel circular hollow sections
Curved beams
Flexural behaviour
Carbon fibre reinforced polymer
Bond length
Failure modes

ABSTRACT

The behaviour of Carbon Fibre Reinforced Polymer (CFRP) strengthened vertically curved beams of Steel Circular Hollow Sections (SCHS) was studied. Sixteen numbers of curved beams with 1200 mm span having four radii of curvatures; 0 mm, 2000 mm, 4000 mm and 6000 mm were tested under three-point bending tests. A range of CFRP lengths up to 1000 mm was selected. The maximum performance was noted when the ratio between CFRP length to total length of beams is 0.625. Four types of failure modes were observed in the strengthened beams. A theoretical model was also developed and validated to predict the load–deflection behaviour of CFRP strengthened tubular vertically curved beams in the elastic region using the Maxwell-Mohr integral method.

1. Introduction

The use of steel tubular sections for civil engineering applications has become popular due to their excellent structural performance and prolonged life spans. Steel hollow sections have high compression, tensile and bending strengths in all directions and have a small drag coefficient in fluid flows. The life span of steel hollow section is longer than other forms of steel sections because of the closed-shape section without sharp corners which reduce the area exposed to outside environment and thus protects the section from corrosion. Moreover, the section void can be filled with concrete to enhance fire protection. The aesthetical appearance and the space provided by the void for installing electric conduits, network cables and other services are advantages of using steel hollow beams in building construction [1]. Beams with Steel Circular Hollow Sections (SCHS) used in construction can be categorized as straight and curved. Hollow section straight members have numerous applications such as in jackets, towers, cranes, bridges, support structures of helicopter decks and further in various secondary structures, such as staircases and ladders. Curved beams can be either bent in the horizontal or vertical plane depending on the application. Beams curved in elevation have structural applications mainly in steel bridges and portals of curved steel roofs. Fig. 1 shows two applications of curved SCHS in a bridge [1] and a roof[2]. During their service lives, structural elements constructed with curved SCHS may become structurally inadequate due to design errors, loss of material properties, exposure to severe environments, or increase in service loads [3]. The present study is limited to SCHS curved in elevation.

Use of Carbon Fibre Reinforced Polymer (CFRP) is a proven retrofitting technique for engineered structures because of CFRP's high durability, superior fatigue endurance, high strength-to-weight ratio, less labour intensive work, and suitability for any sectional shape [3-5]. Many studies have been conducted on the behaviour of CFRP strengthened tubular structures under axial [6-11], bending [3,12-19] and torsional [20,21] loadings. Furthermore, CFRP strengthening of SCHS can enhance durability against transient loadings such as fatigue [22] and impact loadings [23,24] as well as in severe environmental conditions [25-30]. However, only a few studies [31] have investigated the flexural behaviour of hollow steel beams curved in elevation and strengthened with CFRP, and they focussed on square hollow sections. A comprehensive study on the flexural behaviour of CFRP strengthened SCHS beams curved in elevation is therefore required to ensure structural safety, minimize maintenance costs and extend their service lives.

With this in mind, an experimental study was conducted to investigate the flexural behaviour of both CFRP strengthened SCHS beams

* Corresponding author at: Division of Civil Engineering Technology, Institute of Technology, University of Moratuwa, Moratuwa, Sri Lanka.
E-mail address: buddhikacivil@gmail.com (K.A.B. Weerasinghe).

https://doi.org/10.1016/j.engstruct.2021.112040
Received 11 June 2020; Received in revised form 23 January 2021; Accepted 7 February 2021
Available online 14 March 2021

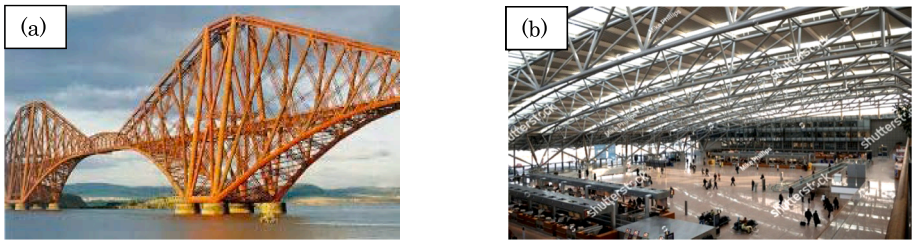

Fig. 1. Structures constructed using SCHS curved in elevation (a) Firth of forth bridge (b) Hamburg airport roof.

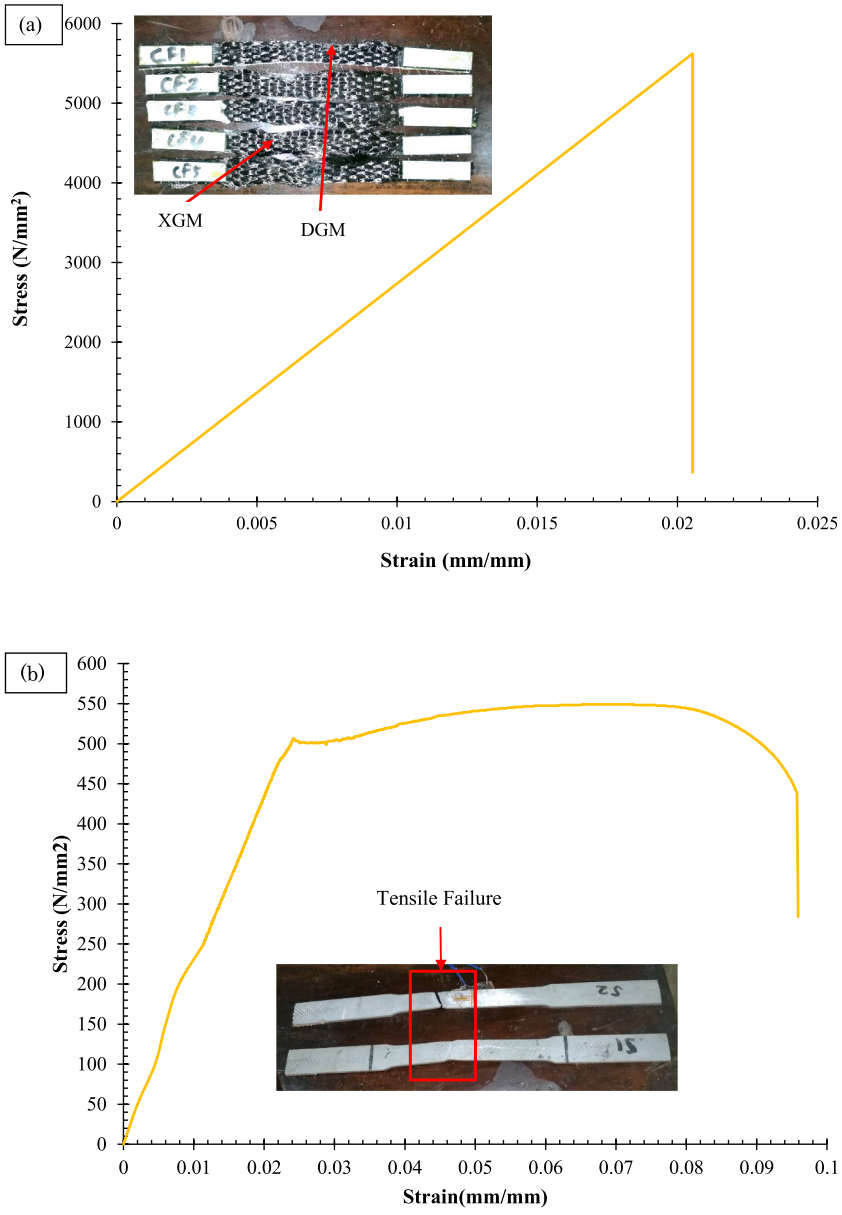

Fig. 2. Stress–strain curves and failure modes of specimens – (a) CFRP and (b) steel.

curved in elevation and straight beams. The effect of curvature of beams and CFRP wrapping lengths on ultimate load carrying capacity, mid span deflection and failure modes were studied. An analytical model was also developed and validated to predict the performance of CFRP retrofitted SCHS beams curved in the vertical plane. The results of the study provide referral guidelines to structural engineers on the practical applications of CFRP to retrofit SCHS curved in elevation.

2. Experimental programme

2.1. Material properties

Coupon tests were conducted according to American Standard Testing Methods to obtain the required material properties for steel (ASTM A:370) [32] and CFRP (ASTM D:3039) [33]. Three steel coupons

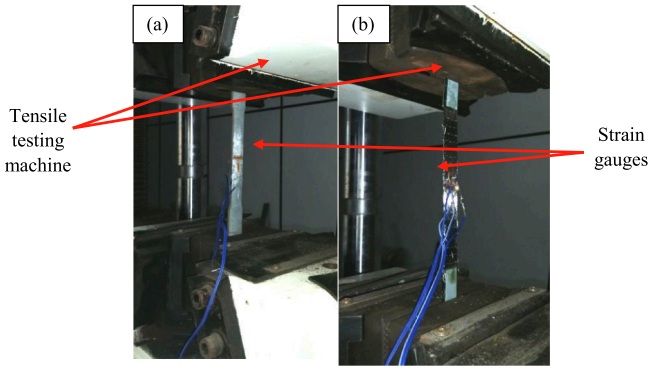

Fig. 3. Coupon tests for (a) steel (b) CFRP.

Table 1
Measured properties of steel, CFRP and epoxy adhesive.

	Steel	CFRP	Epoxy
Thickness (mm)	3	0.116	0.5
Elastic modulus (GPa)	206	230	2.4
Tensile strength (MPa)	473	4983	40
Yield strength (MPa)	508	–	–
Tensile strain (mm/mm)	0.25	0.021	–

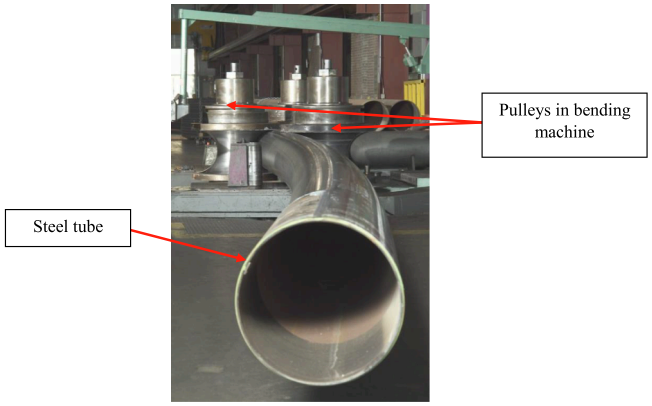

Fig. 4. Bending of steel tubes.

and five CFRP coupons were tested. The stress–strain curves obtained and the failure modes of coupons for CFRP sheets and circular hollow steel tubes are shown in Fig. 2. The failure mode of steel coupon was tensile failure while CFRP showed two major failure modes; edge delamination of the gauge at the middle (DGM) and explosion of the gauge at the middle (XGM). Fig. 3 shows the images taken during the coupon tests for steel and CFRP. Elastic modules in fibre direction (E_1), matrix direction (E_2), and Poisson's ratios in fibre (N_{u12}) and matrix (N_{u13}) directions were obtained during the coupon tests for CFRP. The elastic modulus and Poisson's ratio in third direction were assumed to be

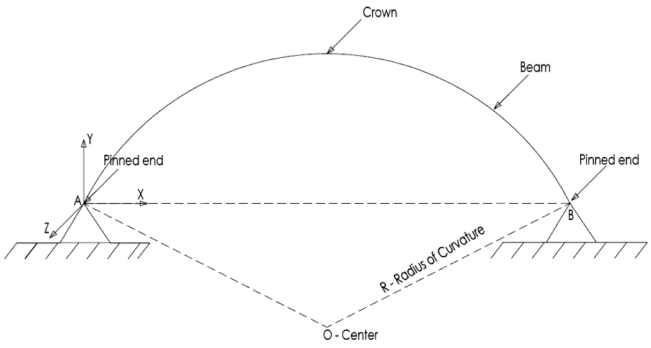

Fig. 6. Description diagram of vertically curved beam.

equal to those of matrix direction for CFRP. Shear modulus for the CFRP in all three directions were obtained using manufacturer provided data. Both elastic and plastic properties for steel and CFRP obtained during the coupon test are listed in Table 1.

2.2. Specimens preparation

A total of 16 samples were prepared using 3 mm thick steel hollow tubes with 101.6 mm outer diameter. The horizontal span of the specimens was kept at a constant value of 1200 mm. Four of these beams were kept as straight beams while the remaining 12 beams were bent (Fig. 4) to have three different radii of 2000 mm, 4000 mm and 6000 mm. Three beams from each radius were strengthened with CFRP and one sample from each category was tested as a control sample.

The surface preparation is of utmost importance to obtain a perfect bond between steel substrate and CFRP patch [3]. As reported in the literature, there are few common methods available to prepare the steel substrate; sand blasting, grit blasting, solvent cleaning and surface grinding [34,35]. Past studies revealed that, grit or sand blasting as the most effective surface preparation method among these [34,36]. Since the current study involves a large surface area to be prepared, a relatively cheap and locally available surface preparation method was required. Sand blasting using garnet abrasive technique was one of the reliable methods and was adopted. The sand blasted surfaces were then cleaned using acetone to remove the loose particles from the surface [37] prior to applying three strain gauges on the bottom surface of the beam one at the mid span and other two at the end positions of the CFRP layer as shown in Fig. 5.

An adhesion promoter was applied on to the prepared surfaces for bonding and kept approximately for one hour for drying before applying the adhesive layer. CFRP sheets were cut into different lengths of 500 mm, 750 mm and 1000 mm with a suitable width such that an overlap of 30 mm exists once they are wrapped on the steel tube. Two parts epoxy adhesive were selected to stick CFRP to the steel [38] and a single layer of CFRP sheet was applied on the adhesive following the wet layup method and immediately a rib roller was run in the longitudinal fibre direction on the CFRP until adhesive and entrapped air bled out. This rib rolling also facilitates to obtain a uniform adhesive layer thickness to avoid stress concentrations. After rolling another layer of adhesive was

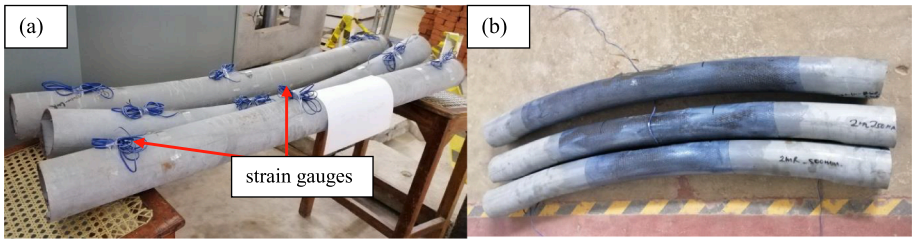

Fig. 5. (a) Un-strengthened (b) strengthened beams.

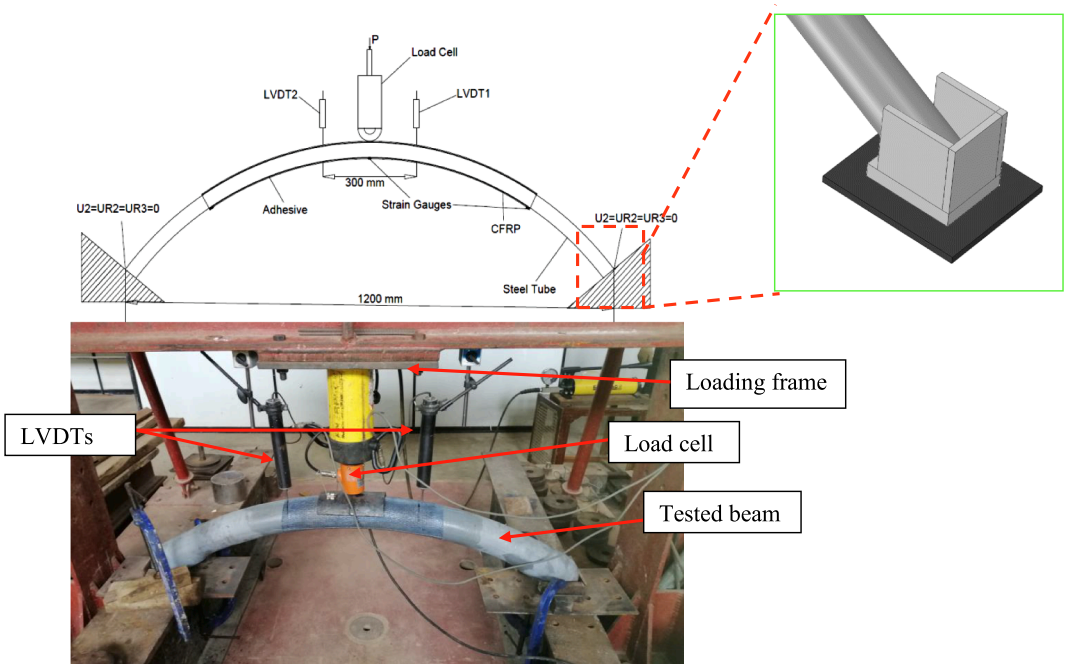

Fig. 7. Test setup and instrumentation.

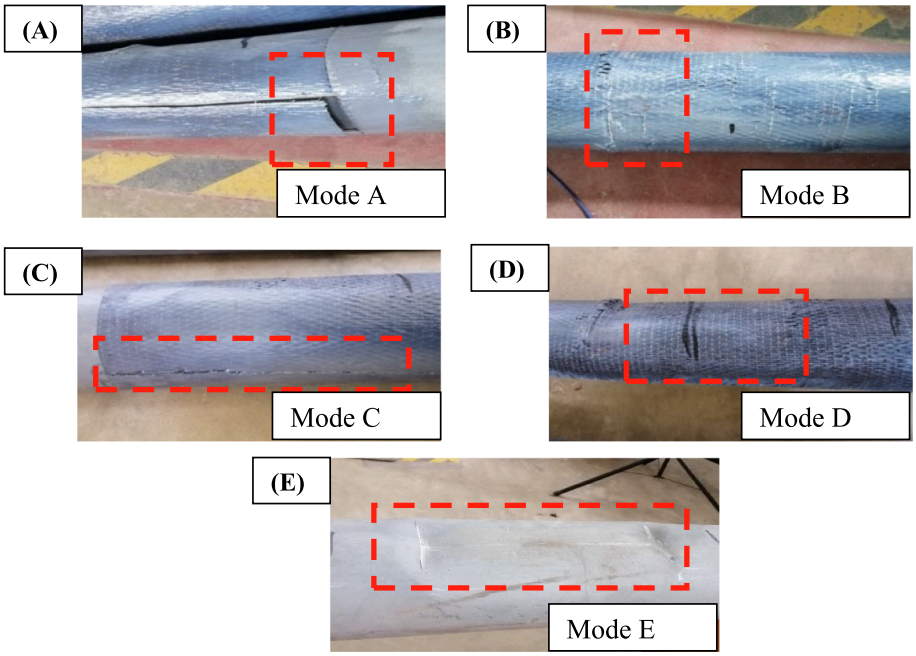

Fig. 8. Major failure modes of tested beams; (A) end debonding (B) CFRP crushing close to the loading point (C) fracture of CFRP at the tensile face opposite side to the load (D) local bucking of steel tube near the loading point (E) Ductile failure of steel tube near the loading point.

applied at either end of the CFRP and also along the overlap to ensure the avoidance of pre-mature debonding failure of CFRP. Fig. 5 shows the specimens prepared before and after applying CFRP. A descriptive diagram of the curved beam is given in Fig. 6.

All the beams were tested under simply supported conditions using three point bending tests in according to the method adopted by previous researchers [39,40]. Tests were conducted using the loading frame available in the structural testing laboratory of University of Moratuwa. A 250 kN capacity load cell was used to transfer the load to the beams at a constant rate of 0.5 mm/min until failure. Two LVDTs were set at 150 mm on either side of the mid span to measure the deflection. Fig. 7 shows the test set up and instrumentation.

3. Experimental results

All un-strengthened and strengthened beams (straight and curved) with various CFRP lengths (0 mm, 500 m, 750 mm and 1000 mm) were tested until failure of CFRP or bearing failure of SCHS. The transient loads and the corresponding deflections and strain variations were noted. The ultimate load of each strengthened beam was compared with that of the corresponding un-strengthened beam. Failure initiation and propagation were also monitored. Furthermore, these failure patterns

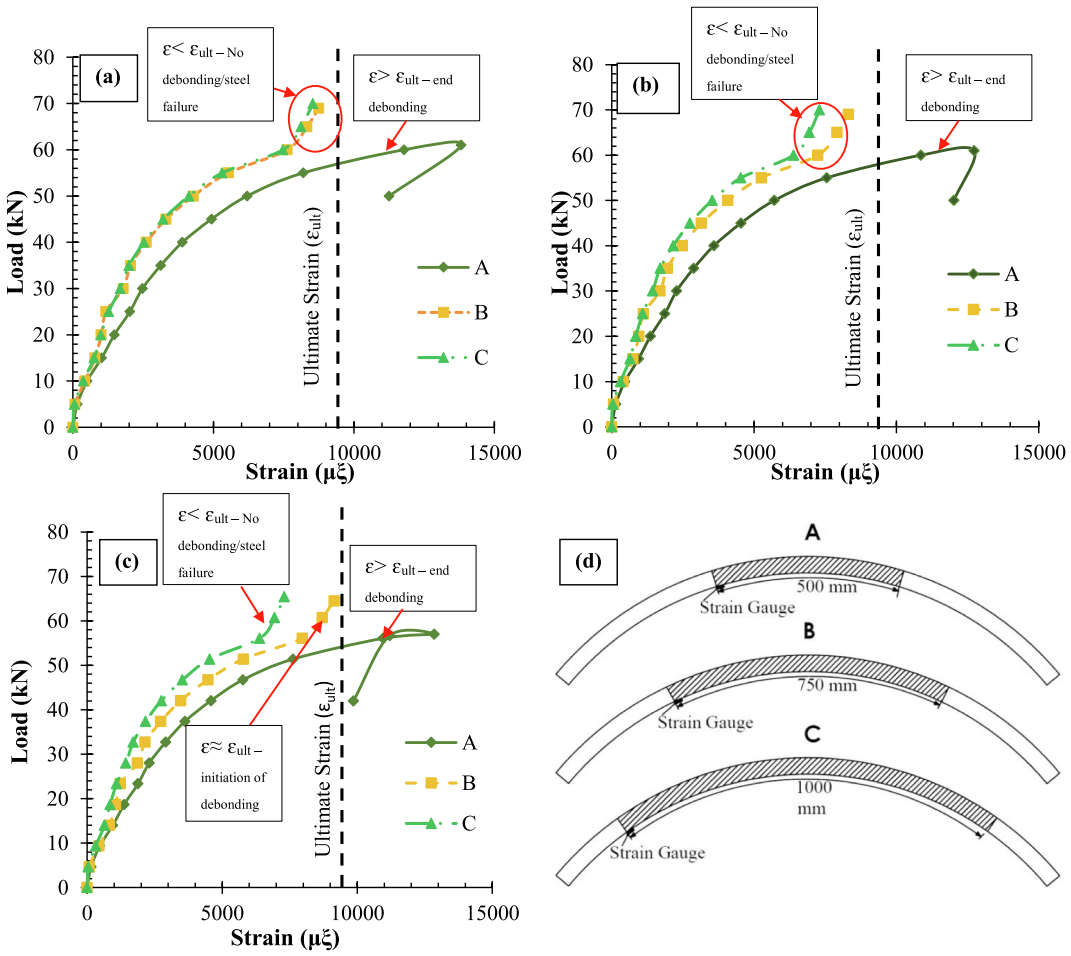

Fig. 9. Variations of strains in adhesive layer for various CFRP lengths for beams with: (a) 2000 mm curvature, (b) 4000 mm curvature' and (c) 6000 mm curvature and (d) positions of strain gauges.

were used to validate the theoretical predictions.

3.1. Failure mechanisms

The four major failure modes observed in both un-strengthened and strengthened beams with different curvatures and different CFRP lengths are shown in Fig. 8 and are discussed as follows. All un-strengthened beams exhibited the failure mode of local buckling (Mode E) near the loading point at the compression zone, irrespective of curvature. Beams with 500 mm long CFRP failed due to end debonding following the rupture in the fibre direction irrespective of the radius of curvature. This failure can be due to the high stress concentration developed at the ends of CFRP layers which could not be withstood by the adhesive. For beams with CFRP length 750 mm, a slight debonding

Table 2
Details of test specimens, ultimate loads and failure modes.

Beam ID	Radius of Curvature (mm)	CFRP Length (mm)	P_u (kN)	(P_u/P_s)%	δ_u(mm)	δ_u/δ_s	Failure Mode
ST_0	0	0	40.2	–	19.2	1.0	C
ST_500		500	41.5	3	23.0	1.2	A/B
ST_750		750	51.6	28	35.1	1.8	A/C/D
ST_1000		1000	52.7	31	31.6	1.6	C/D
2R_0	2000	0	56.2	–	29.7	1.0	C
2R_500		500	61.2	9	24.3	0.8	A/B
2R_750		750	70.0	24	41.2	1.4	A/C/D
2R_1000		1000	68.9	23	40.4	1.4	C/D
4R_0	4000	0	52.9	–	25.8	1.0	C
4R_500		500	55.6	5	24.5	0.9	A/B
4R_750		750	63.3	20	33.1	1.3	A/C/D
4R_1000		1000	60.9	15	36.1	1.4	C/D
6R_0	6000	0	48.8	–	28.3	1.0	C
6R_500		500	51.6	6	27.6	1.0	A/B
6R_750		750	55.8	14	35.1	1.2	A/C/D
6R_1000		1000	55.0	12	31.2	1.1	C/D

In Table 2, the failure modes are denoted as: A – CFRP end debonding; B – CFRP rupture in tensile face; C- Local buckling of tube near loading point; D – CFRP rupture close to loading point and ultimate loads and mid span deflections at ultimate loads are denoted as; P_u – ultimate load of strengthened beams; P_s – Ultimate load on un-strengthened beam; δ_u – mid span deflection at ultimate for strengthened beams; δ_s – mid span deflection at ultimate for un-strengthened beams.

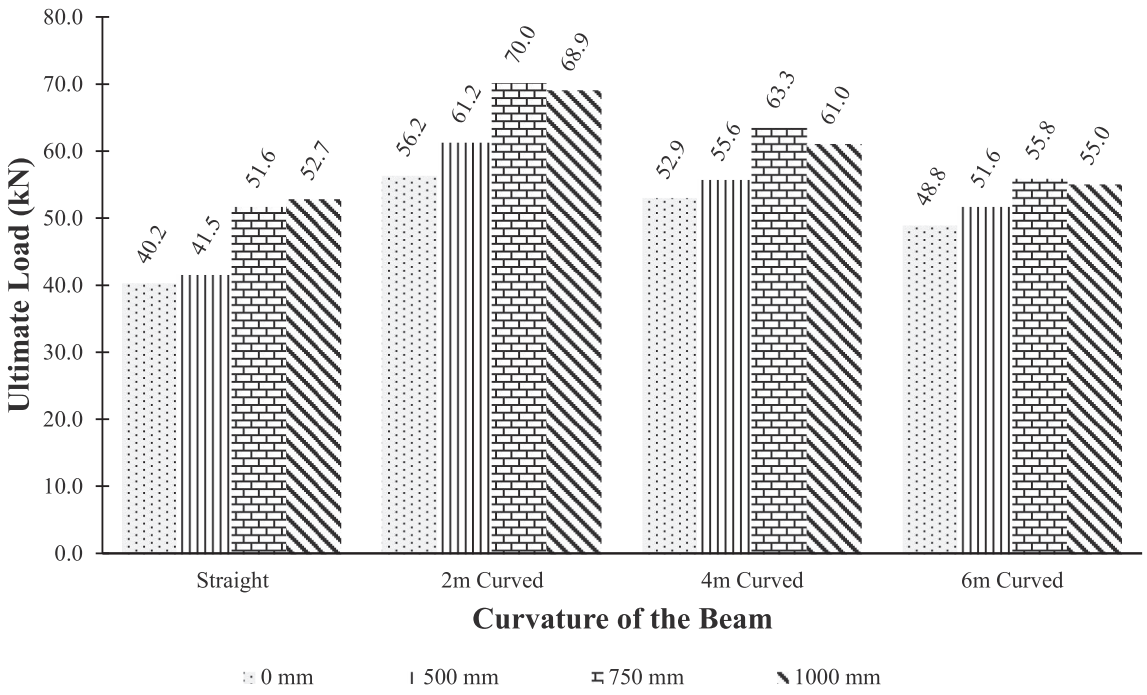

Fig. 10. Variation of ultimate load with CFRP Length for beams with different radii of curvature.

at the ends of the CFRP was observed. Then local buckling started in the SCHS near the loading point at the compression zone following the CFRP fibre rapture near the same area. No end debonding failure was observed for the beams with 1000 mm long CFRP sheets. Those beams failed due to local buckling of SCHS near the loading point which led to the CFRP fibre rupture. It can therefore be deduced that the failure modes of strengthened beams were governed by the length of the CFRP which had an effect on the different strain levels within the adhesive. Fig. 8 shows the variation of strain within the adhesive at the edges of CFRP layer for various CFRP lengths for beams with 2000 mm radius of curvature. It clearly indicates that strain levels of the adhesive exceed its ultimate strain value before failure in beams with 500 mm long CFRP. Therefore, CFRP debonding has occurred in these beams. However, for the beams with 750 mm and 1000 mm CFRP lengths the strain in the adhesive does not exceed its ultimate value before local buckling of steel tube occurs and hence no debonding could be observed.

It was observed that the failure modes of both un-strengthened and strengthened beams were not influenced by the curvature of the beam, instead they depended only on the length of CFRP wrapping.

3.2. Strain variations

Fig. 9 shows the strain variations in the adhesive at the edge of CFRP layer, for CFRP strengthened curved beams with different curvatures and CFRP lengths. It clearly indicates that the strains in the beam with 500 mm CFRP lengths exceed the ultimate strain (ε_{ult}) in adhesive. This causes the debonding of CFRP sheet. For the beam of 6000 mm curvature with 750 mm long CFRP, strain in adhesive attained a value close to the ultimate value and hence slight debonding is observed. This was not observed in beams with 2000 mm and 4000 mm curvatures. However, for beam with 1000 mm CFRP length adhesive strain was well below the adhesive ultimate strain and hence no debonding is observed in that beam [13,41]. The strain variations in Fig. 9(b) and Fig. 9(c) for beams with 4000 mm curvature and 6000 mm curvature respectively, show

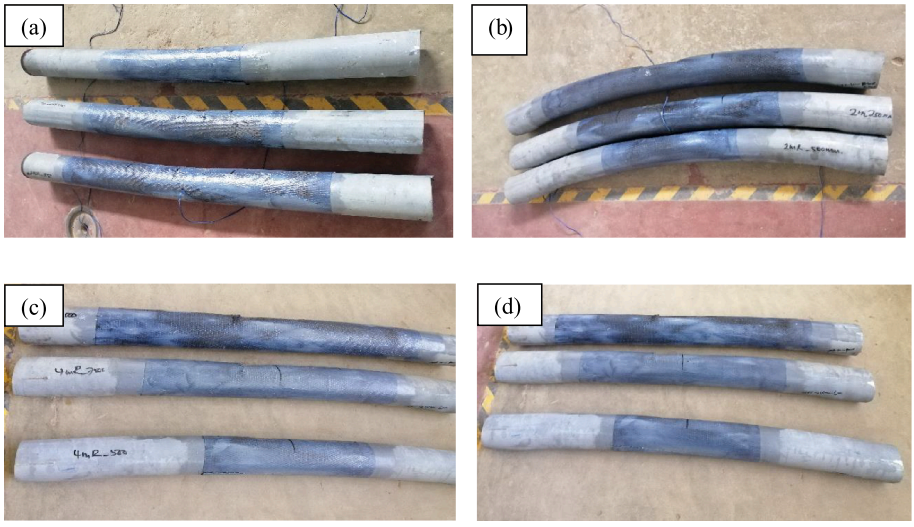

Fig. 11. Deflected shapes of strengthened beams with different radii R and CFRP lengths (a) straight (b) 2000 mm (c) 4000 mm and (d) 6000 mm radii.

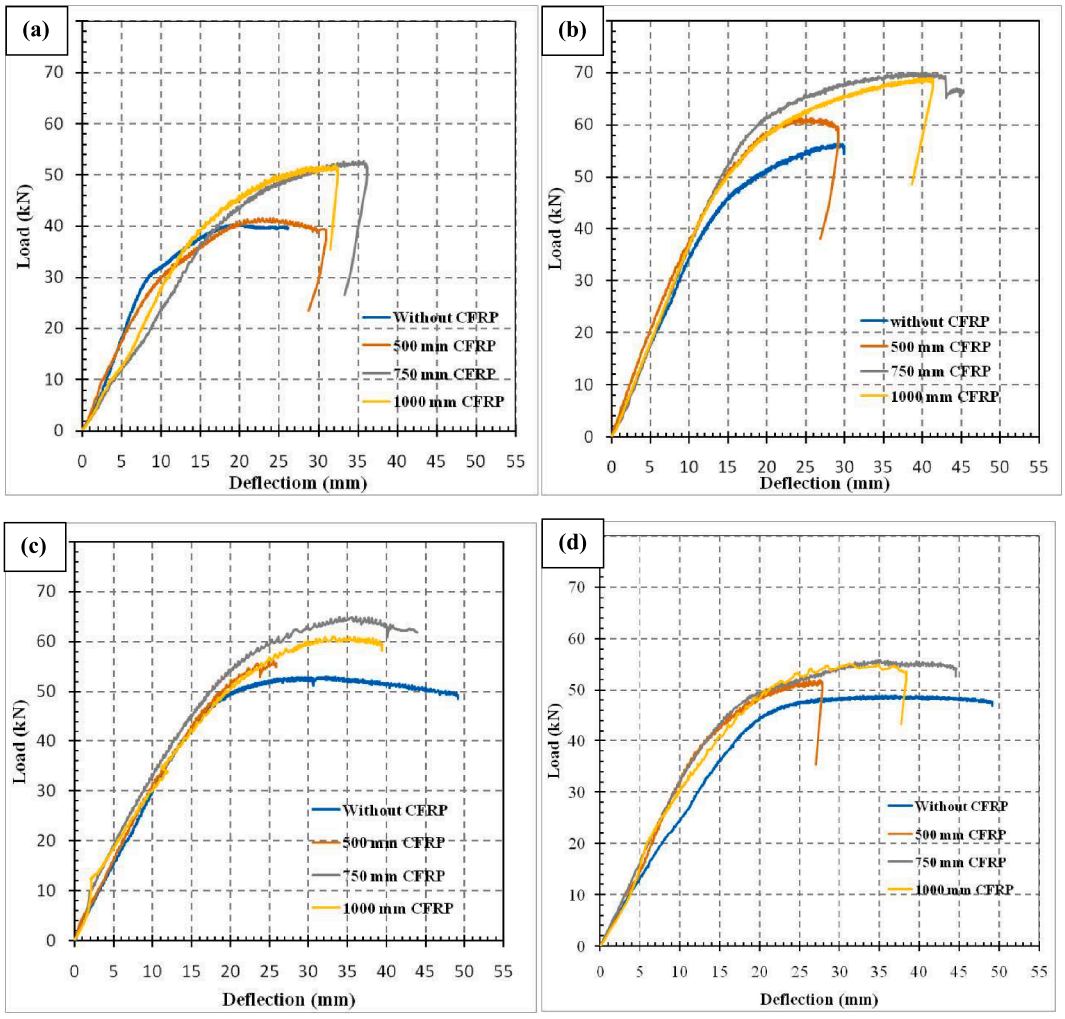

Fig. 12. Load-deflection curves for curved beams with different radii of curvature and CFRP-bonded lengths: (a) straight beam, (b) 2 m curved beam, (c) 4 m curved beam, and (d) 6 m curved beam.

identical variations of strains compared to beams with 2000 mm curvature. Ultimate strain in adhesive is also shown in each diagram.

3.3. Failure Loads.

Table 2 shows the ultimate loads, strength gain and failure mechanisms of both strengthened and un-strengthened beams. It is clearly observed that the ultimate load increases when CFRP length increases in straight beams while the ultimate load increases up to 750 mm CFRP length and a slight reduction was appeared when the length is 1000 mm. This may due to the inefficient load transfer to CFRP due to the relatively larger distance from the loading point.

The highest load carrying capacities of un-strengthened beams were observed in curved beams with radius of 2000 mm. When the radius of curvature increases the ultimate loads were observed to be reduced. Compared to straight un-strengthened beams the percentage increments of ultimate loads for beams with 2000 mm, 4000 mm and 6000 mm radii were 40%, 32% and 21%, respectively.

The highest load increment was observed in straight beams with 1000 mm long CFRP. The highest load at 52.7 kN is an increase of 31% compared to that in the un-strengthened beam. For straight beams with 500 mm and 750 mm CFRP lengths the percentage load increments compared to the bare (un-strengthened) beam were 3% and 28%, respectively. Fig. 10 shows the failure (ultimate) loads observed in the tested beams. The highest load increment for 750 mm CFRP was observed in beams with 2000 mm radius and is 24% which is 5% greater than that in beams with 4000 mm radius of curvature and 10% greater than beams with 6000 mm radius of curvature. The highest percentage increases of 9%, 24% and 23% in the ultimate loads occurred in the beams of 2000 mm radius with 500 mm, 750 mm and 1000 mm CFRP lengths respectively. Of the curved beams, the lowest tensile stress developed within the tensile face of the beam with the highest radius and this value is slightly lesser than that in the straight beams. This variation might be due to the reduction in residual stress caused by beam bending [42]. The strengthened curved beams showed similar trends of strength gain irrespective of the beam curvature.

Fig. 11 shows the final deflected shapes of beams with various curvatures and CFRP lengths. It can be seen that the deflected shapes of all these beams show the same trend. For curved beam with 2000 mm radius, some curvature is evident in the deflected beam even after failure. For the straight beams final deflected shape indicates negative curvature while beams with 4000 mm and 6000 mm radii seem almost straight.

3.4. Mid span deflection

Load-deflection responses of both un-strengthened and strengthened beams for each radius of curvature and CFRP length are given in Fig. 12. All the strengthened beams show a higher stiffness than the un-strengthened beams within both elastic and plastic limits. This

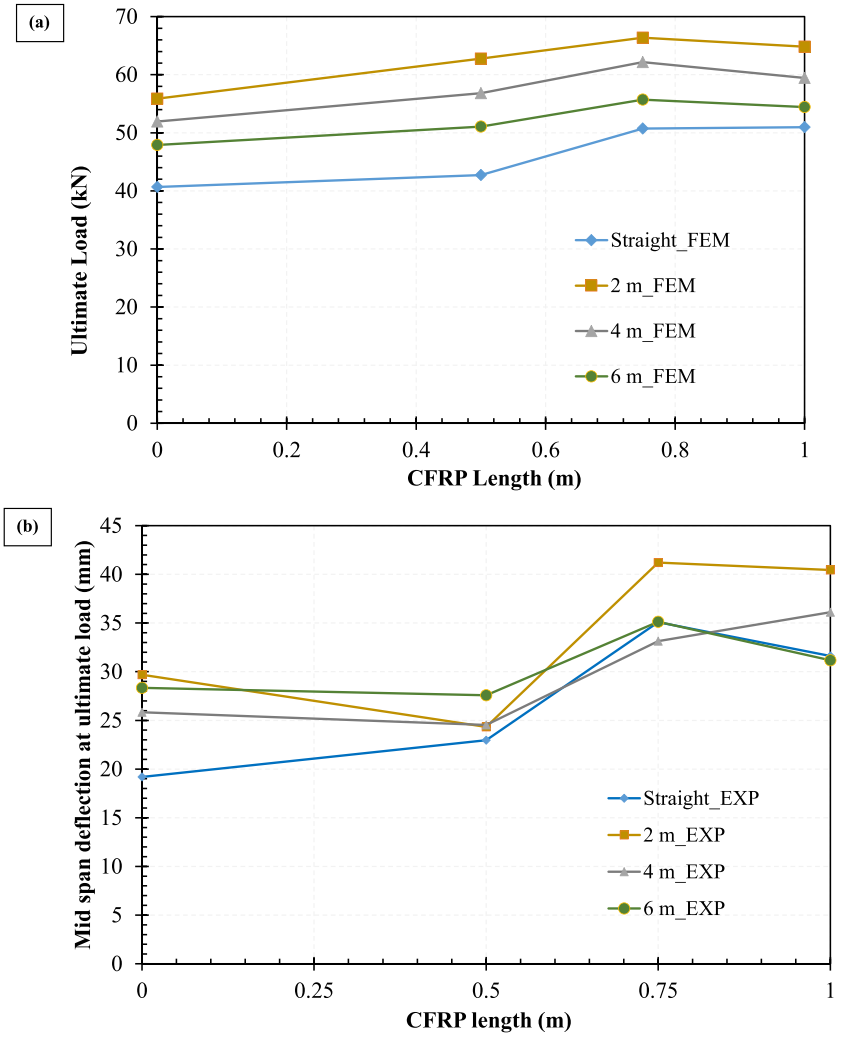

Fig. 13. Variation of (a) ultimate load (b) mid span deflection at ultimate loads for various CFRP lengths for curved beams.

variation in stiffness was highlighted more within the plastic region. It can be clearly seen that the deflections at failure for strengthened beams with 750 mm and 1000 mm CFRP lengths are greater than those of un-strengthened beams. Beams with 500 mm CFRP lengths show lower deflections at failure compared to un-strengthened beams due to premature deboning of CFRP for all tested beams irrespective from their radii. Until40 kN load level, deflections of strengthened 2000 mm radius curved beams were almost the same. These curved beams strengthened with 750 mm and 1000 mm CFRP lengths show 39% and 35% increase in deflections respectively at ultimate load. Strengthened beams with 4000 mm and 6000 mm radii show the same trend, but the deflections were close to each other only up to a load of 30 kN. Highest increments of 20%, 83% and 65% in mid span deflections at ultimate loads were observed in straight beams with 500 mm, 750 mm and 1000 mm CFRP lengths, respectively.

Variation of the experimental ultimate load with CFRP wrapping length for each beam with different curvature is shown in the Fig. 13(a). It clearly shows that for each CFRP length, the maximum ultimate load was found in 2000 mm radius curved beam. Ultimate loads of beams for each CFRP length gradually decreases when the radius of the beam increases. For each beam ultimate load capacity increases until CFRP length increases to 750 mm and a small reduction was noted when CFRP length greater than 750 mm. Therefore, it can be deduced that the ultimate loads for a strengthened beam attains the highest value when CFRP length is750 mm. At this point the ratio between the CFRP length to total length of beam is 0.625.

Fig. 13(b) shows the variation between mid- span deflection with respect to CFRP length for beams with different radii. It can be clearly seen that the highest mid span deflections for 750 mm and 1000 mm CFRP lengths were observed in 2000 mm radius curved beams. For straight beams and 6000 mm radius curved beams, deflections for 750 mm and 1000 mm CFRP lengths are almost the same. Except 4000 mm radius curved beams, the maximum deflections at ultimate load occurred in the beams with 750 mm CFRP length. All the beams showed the same trends for ultimate loads and mid span deflection for various CFRP lengths.

Mid span deflections at ultimate loads for beams with different radii and CFRP lengths presented in Table 2. For beam with 6000 mm radius and 500 mm CFRP, deflection at ultimate load is smaller compared to the un-strengthened beam. The deflections at the ultimate load for straight beams and 4000 mm radius curved beams have increased irrespective of CFRP length. For the 2000 mm curved beam, the mid span deflection at the ultimate load for 500 mm CFRP length is less compared to un-strengthened beam, but it increases for 750 mm and 1000 mm CFRP lengths.

4. Analytical study

In this section an analytical model for curved steel tubular beams strengthened with CFRP is proposed using Maxwell-Mohr integral.

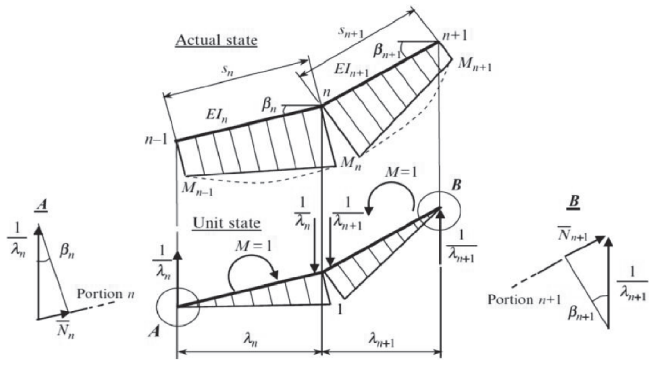

S_n - Length of the nth section

M_n - Bending moment at nth node

E - Elastic modulus of beam material

I_n - Moment of inertia for nth section

β_n - Horizontal inclination of nth section

λ_n- Vertical projection of axial force of nth section

Fig. 14. Loads acting on left and right portion.

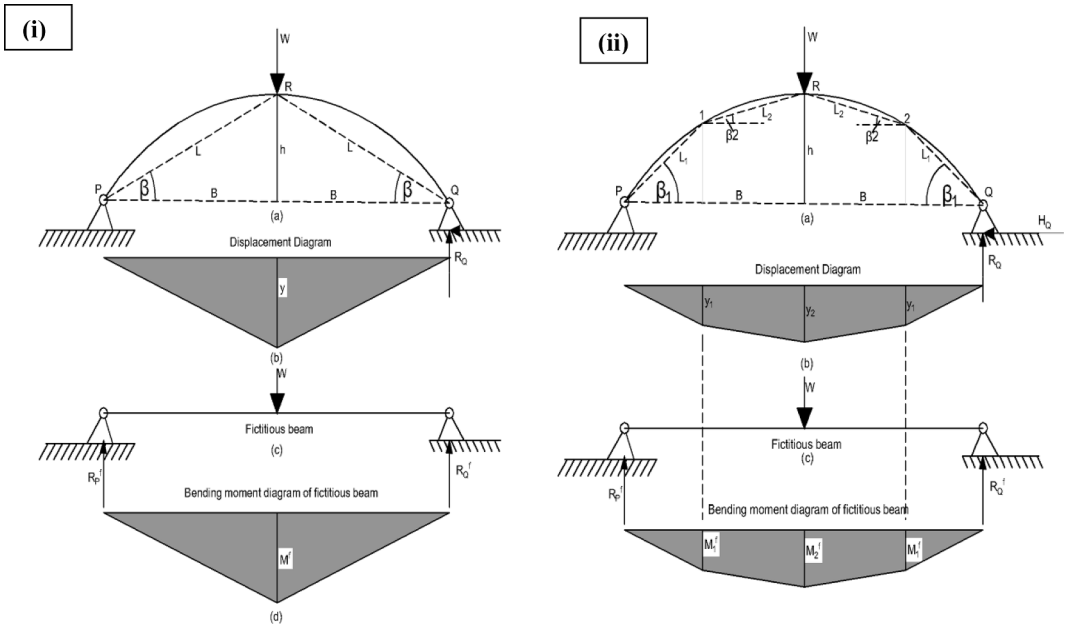

Fig. 15. Curvilinear simply supported bar. (i) un-strengthened beam (ii) strengthened beam with; (a) Design diagram; (b) vertical displacements; (c) fictitious beam; (d) corresponding bending moment diagram.

Elastic deformations of un-strengthened and strengthened curved beams were evaluated using the conjugate beam method presented in the literature [36]. This method was developed considering not only the bending moment but also the axial force developed in curved beams. Fig. 13 shows two inclined parts of a beam with lengths S_n and S_{n+1} are subjected to bending moments and axial forces. By assuming the axial forces $\overline{N}_n$ and $\overline{N}_{n+1}$ are constants, axial forces in the unit states are $\overline{N}_n = -sin\beta_n/\lambda_n$ and $\overline{N}_{n+1} = -sin\beta_{n+1}/\lambda_{n+1}$ for the left and right portions respectively. Calculation of these forces are shown in Fig. 14, at joints A and B.

For left portion using Maxwell and Mohr integral [44] for bending moment will give the elastic load on the beam due to bending moment

$$W_n(M) = \sum \int_0^l \overline{M}\frac{M_p}{EI}dx = \frac{s_n}{6EI_n}(2M_{n-1}\times 0 + 2M_n \times 1 + M_{n-1}\times 1 + M_n \times 0) = \frac{s_n}{6EI_n}(M_{n-1} + 2M_n) \quad (1)$$

where M_p is the bending moment at the nth node due to vertical loads and $\overline{M}$ is the bending moment in the unit state. EI_n is the flexural rigidity of the beam portion considered.

By using Maxwell and Mohr integral for axial force will give the elastic load on the beam due to axial force $W_n(N)$;

$$W_n(N) = \sum \int_0^l \overline{N}\frac{N_p}{EA}dx = -\frac{1}{EA_n}\times\frac{\sin\beta_n}{\lambda_n}N_nS_n = -\frac{1}{EA_n}\times\frac{\sin\beta_n}{\lambda_n}N_n\frac{\lambda_n}{\cos\beta_n} = \frac{N_n}{EA_n}\times\tan\beta_n \quad (2)$$

where N_p is the axial force at the nth node due to vertical loads and $\overline{N}$ is the axial force in the unit state. E is the elastic modulus of the beam portion considered and A is the cross sectional area of the beam.

Then the total elastic load on the beam is given by;

$$W_n = W_n(M) + W_n(N) \quad (3)$$

Substituting to (3) from (1) and (2) gives;

$$W_n = \frac{S_n}{6EI_n}(M_{n-1} + 2M_n) + \frac{S_{n+1}}{6EI_{n+1}}(2M_n + M_{n+1}) - \frac{N_n}{EA_n}\tan\beta_n + \frac{N_{n+1}}{EA_{n+1}}\tan\beta_{n+1} \quad (4)$$

For un-strengthened beam shown in Fig. 15(i);
But,

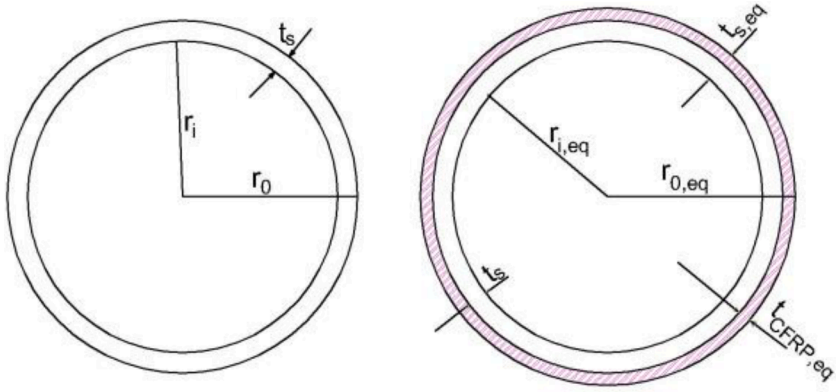

Fig. 16. Section of steel tube (a) un-strengthened beam; (b) strengthened equivalent section.

$$s_n = s_{n+1} = L, I_n = I_{n+1} = I, A_n = A_{n+1} = A, \beta_n = \beta_{n+1} = \beta, M_{n-1} = M_{n+1} = 0, M_n = \frac{WB}{2},$$

$$N_n = N_{n+1} = W/2\sin\beta$$

Substituting these values in (4) gives;

$$W_n = \frac{L}{6EI}\left(0 + 2\frac{WB}{2}\right) + \frac{L}{6EI}\left(2\frac{WB}{2} + 0\right) - \frac{W}{2EA}\frac{\tan\beta}{\sin\beta} - \frac{W}{2EA}\frac{\tan\beta}{\sin\beta}$$

$$W_n = \frac{WLB}{3EI} - \frac{W}{EA}\frac{1}{\cos\beta} \tag{5}$$

$$R_P^f = R_Q^f = \frac{W_n}{2}$$

$$M^f = y = R_P^f \times B = \frac{WB}{3EI}\left(LB - \frac{3I}{A\cos\beta}\right) \tag{6}$$

For Strengthened beams;

$$W_n(M) = \frac{s_n}{6EI_n}(M_{n-1} + 2M_n) + \frac{s_{n+1}}{6EI_{n+1}}(M_{n+1} + 2M_n) \tag{7}$$

$$W_n(N) = -\frac{N_n}{EA_n}\tan\beta_n + \frac{N_{n+1}}{EA_{n+1}}\tan\beta_{n+1} \tag{8}$$

By applying above (7) and (8) for the strengthened beam shown in Fig. 15(ii);

For the PR section;

$$W_1(M) = \frac{L_1}{6EI}(0 + 2M_1) + \frac{L_2}{6EI_{eq}}(M_R + 2M_1) \tag{9}$$

$$W_1(N) = -\frac{N}{EA}\tan\beta_1 + \frac{N}{EA_{eq}}\tan\beta_2 \tag{10}$$

$$W_1 = \frac{L_1}{3EI}(M_1) + \frac{L_2}{6EI_{eq}}(M_R + 2M_1) + -\frac{N}{EA}\tan\beta_1 + \frac{N}{EA_{eq}}\tan\beta_2 \tag{11}$$

For the section 1–2 in Fig. 14(ii);

$$W_2(M) = \frac{L_2}{6EI_{eq}}(M_1 + 2M_R) + \frac{L_2}{6EI_{eq}}(M_2 + 2M_R) \tag{12}$$

Since $M_1 = M_2$;

$$W_2(M) = \frac{L_2}{3EI_{eq}}(M_1 + 2M_R) \tag{13}$$

$$W_2(N) = -\frac{N}{EA_{eq}}\tan\beta_2 - \frac{N}{EA_{eq}}\tan\beta_2 = -\frac{2N}{EA_{eq}}\tan\beta_2 \tag{14}$$

$$W_2 = \frac{L_2}{3EI_{eq}}(M_1 + 2M_R) - \frac{2N}{EA_{eq}}\tan\beta_2 \tag{15}$$

It is obvious that $W_1(M) = W_3(M)$ and $W_1(N) = W_3(N)$, where $W_1(M)$ is the $W_n(M)$ for section RQ and $W_3(N)$ is $W_n(N)$ for section RQ.

$$W_n(M) = 2\left[\frac{L_1}{6EI}.(2M_1) + \frac{L_2}{6EI_{eq}}(M_R + 2M_1)\right] + \frac{L_2}{3EI_{eq}}(M_1 + 2M_R) \tag{16}$$

$$W_2 = \frac{L_2}{3EI_{eq}}(M_1 + 2M_R) - \frac{2N}{EA_{eq}}\tan\beta_2 \tag{17}$$

Total Elastic load on the beam is given by;

$$W_n = \frac{2L_1M_1}{3EI} + \frac{L_2}{EI_{eq}}(M_1 + M_R) - \frac{2N}{EA}\tan\beta_1 \tag{18}$$

Elastic reaction at the support $R_P^f$is given by;

$$R_P^f = R_Q^f = \frac{W_n}{2} \tag{19}$$

Therefore, the deflection at the crown due to a elastic load W;

$$M^f = y = R_P^f \times B = \frac{B}{2}\left[\frac{2L_1M_1}{3EI} + \frac{L_2}{EI_{eq}}(M_1 + M_R) - \frac{2N}{EA}\tan\beta_1\right] \tag{20}$$

where M_1 is the bending moment at point 1 and M_R is the bending moment at point R due to vertical reaction. y is the vertical displacement at the crown of the beam.

The equivalent second moment of area for the cross section of strengthened part can be calculated as follow (Fig. 16).

For the un-strengthened beam assuming steel tube as a thin walled section;

$$I = \pi r_0^3 t_s \tag{21}$$

where I is the second moment of area, r_0 is the radius of and t_s is the wall thickness of unstrengthened section.

The second moment of area of the equivalent section I_{eq} is given by;

$$I_{eq} = \pi r_{eq}^3 t_{eq} \tag{22}$$

where r_{eq} and t_{eq} can be found by Eqs. (20) and (19) respectively.

$$t_{eq} = t_s + t_{CFRP,eq} \tag{23}$$

$$r_{eq} = r_0 + t_{CFRP,eq} \tag{24}$$

$$t_{CFRP,eq} = \frac{E_s}{E_{CFRP}} \times t_{CFRP} \tag{25}$$

In Eq. (24) $t_{CFRP,eq}$ is found by Eq. (25).

When evaluating the total deflection at the mid span, the ovalisation

Table 3
Comparison between experimental results and analytical model.

Beam ID	Radius of Curvature (mm)	CFRP Length (mm)	Elastic Load Considered (kN)	Experimental deflection (δ_{exp}) (mm)	Analytical deflection (δ_{al}) (mm)	Total analytical deflection including ovalisation ($\Delta_T = \delta_{al} + 3$)	Δ_T/δ_{exp}
2R_0	2000	0	40	13.02	11.1	14.1	1.08
2R_500		500	40	10.20	7.02	10.02	0.98
2R_750		750	40	10.20	7.56	10.56	1.04
2R_1000		1000	40	10.18	7.86	10.86	1.07
4R_0	4000	0	30	10.20	8.55	11.55	1.13
4R_500		500	30	9.15	5.41	8.41	0.92
4R_750		750	30	9.00	5.83	8.83	0.98
4R_1000		1000	30	9.54	6.05	9.05	0.95
6R_0	6000	0	30	12.00	8.60	11.60	0.97
6R_500		500	30	9.22	5.58	8.58	0.93
6R_750		750	30	9.15	5.85	8.85	0.97
6R_1000		1000	30	9.65	6.08	9.08	0.94

of SCHS due to the applied load should be considered. Researchers [43,45] have found that the ovalisation depends on the aspect ratio (ratio between diameter and thickness) of the section. According to those researchers, for SCHS having aspect ratio of around 33, the percentage ovalisation was about 5% at the ultimate load. For this study since the elastic limit is considered, it is effective to use a percentage ovalisation of 3%. Since the diameter of the circular hollow sections used in this is 101.6 mm, it is conservative to take amount of ovalisation as 3 mm. Therefore, the total deflection (Δ_T) can be expressed as;

$$\Delta_T = \delta_{al} + \delta_{ol} \tag{26}$$

The calculated deflections of the strengthened and unstrengthened beams with different radii of curvature under elastic loads of 40 kN and 30 kN are shown in Table 3. By comparing the analytical model results and experimental results, it was found that the results are in good agreement. Therefore, the developed analytical model based on the Maxwell-Mohr integration can be used effectively to calculate the deflection at a given elastic load or load at a given deflection for CFRP strengthened vertical curved tubular sections.

5. Conclusions

An experimental study was conducted to investigate the behaviour of vertically curved tubular steel members strengthened with CFRP. An analytical study was also conducted to evaluate the deflection of both strengthened and un-strengthened beams in the elastic range. Based on the experimental and analytical studies, the following conclusions can be drawn;

- CFRP is an efficient material to strengthened curved steel hollow sections since, it increases the load carrying capacity of the beams and reduces the deflection of the beam at any given load. Maximum ultimate strengths of the CFRP retrofitted curved SCHS were obtained when the ratio of CFRP length to the total length of beam becomes 0.625. Ultimate strengths were observed to be lower for the values of this ratio less than or greater than 0.625.
- The highest load carrying capacities for all CFRP wrapping lengths were observed for beams with 2000 mm radius of curvature and the lowest values were observed in straight beams. This clearly indicates that the ultimate load carrying capacity of a curved SCHS for a certain CFRP wrapping length decreases when radius of curvature of the beam increases. Strengthening of SCHS using CFRP reduces the amount of mid span deflection at the ultimate load. The highest mid span deflections among all curved beams with different CFRP lengths were observed for those with a radius of 6000 mm. When the radius of curvature decreases the mid span deflection also decreases. The highest deflections at the ultimate load for strengthened beams with various curvatures were observed when the ratio between CFRP length to total length of the beam equals to 0.625.
- Four major failure types were observed in CFRP strengthened curved SCHS beams which include debonding of CFRP due to adhesive failure, bearing of the steel tube near the loading point, crushing of CFRP near the loading point and CFRP rupture on the tension face of the beam. When CFRP wrap length was 500 mm the major failure mechanism of beams was pre- mature debonding of CFRP. Beams strengthened with 500 mm CFRP also showed rupture of CFRP at lower loads. When CFRP length increased to 750 mm and 1000 mm, failure mechanisms of beams were fracture of CFRP and bearing of the steel tube near the loading point.
- A method to analyse CFRP strengthened SCHS under elastic loads was developed according to Maxwell-Mohr integral method (and validated). This method can evaluate the deflection at a given elastic load or the load for a given elastic deflection.

Declaration of Competing Interest

The authors declare that they have no known competing financial interests or personal relationships that could have appeared to influence the work reported in this paper.

Acknowledgement

The authors wish to extend their gratitude to the University of Moratuwa (UoM) for providing financial support to carry out the work reported in this paper under the SRC grant SRC/LT/2019/21.

References

[1] Wardenier J. HOLLOW SECTIONS Hollow Sections in Structural Applications, Technology; 2001. p. 199.
[2] Hamburg airport roof. [Online]. Available: https://www.shutterstock.com/image-photo/hamburg-airport-roof-26921713. [Accessed: 25-Apr-2020].
[3] Kabir MH, Fawzia S, Chan THT, Gamage JCPH, Bai JB. Experimental and numerical investigation of the behaviour of CFRP strengthened CHS beams subjected to bending. Eng Struct 2016;113:160–73.
[4] Zhao XL, Zhang L. State-of-the-art review on FRP strengthened steel structures. Eng Struct 2007;29(8):1808–23.
[5] Teng JG, Yu T, Fernando D. Strengthening of steel structures with fiber-reinforced polymer composites. J Constr Steel Res 2012;78:131–43.
[6] Gao XY, Balendra T, Koh CG. Buckling strength of slender circular tubular steel braces strengthened by CFRP. Eng Struct 2013;46:547–56.
[7] Sundarraja MC, Sriram P, Ganesh Prabhu G. Strengthening of hollow square sections under compression using FRP composites. Adv Mater Sci Eng 2014;2014.
[8] Keykha AH, Nekooei M, Rahgozar R, Narmashiri K. Investigation of load increment in hollow steel short and slender columns strengthened using CFRP. WALIA J 2015;31(S3):163–9.
[9] Devi U, Amanat KM. Non-linear finite element investigation on the behavior of CFRP strengthened steel square HSS columns under compression. Int J Steel Struct 2015;15(3):671–80.
[10] Teng JG, Hu YM. Behaviour of FRP-jacketed circular steel tubes and cylindrical shells under axial compression. Constr Build Mater 2007;21(4):827–38.

[11] Shaat A, Fam A. Axial loading tests on short and long hollow structural steel columns retrofitted using carbon fibre reinforced polymers. Can J Civ Eng 2006;33 (4):458–70.
[12] Teng JG, Fernando D, Yu T. Finite element modelling of debonding failures in steel beams flexurally strengthened with CFRP laminates. Eng Struct 2015;86:213–24.
[13] Badawy A, Abu-sena B, Said M, Zaki MA, Dokmak M. Behavior of hollow steel sections strengthened with CFRP. Constr Build Mater 2019;205:306–20.
[14] Elchalakani M. CFRP strengthening and rehabilitation of degraded steel welded RHS beams under combined bending and bearing. Thin-Walled Struct 2014;77: 86–108.
[15] Zhao O, Rossi B, Gardner L, Young B, Asce M. Experimental and numerical studies of ferritic stainless steel tubular cross sections under combined compression and bending. J Struct Eng ASCEng 2015.
[16] Fawzia S, Al-Mahaidi R, Zhao XL, Rizkalla S. Strengthening of circular hollow steel tubular sections using high modulus CFRP sheets. Constr Build Mater 2007;21(4): 839–45.
[17] Haedir J, Bambach MR, Zhao XL, Grzebieta RH. Strength of circular hollow sections (CHS) tubular beams externally reinforced by carbon FRP sheets in pure bending. Thin-Walled Struct 2009;47(10):1136–47.
[18] Babu BR, Sundarraja MC. Strengthening of Square Hollow Structural Steel (Hss) Tubular Sections Using Cfrp Strips. pp. 25–34.
[19] Zhou Y, et al. Experimental flexural behaviors of CFRP strengthened aluminum beams. Compos Struct 2014;116(1):761–71.
[20] Abdollahi Chahkand N, Zamin Jumaat M, Ramli Sulong NH, Zhao XL, Mohammadizadeh MR. Experimental and theoretical investigation on torsional behaviour of CFRP strengthened square hollow steel section. Thin-Walled Struct 2013;68:135–40.
[21] Wu C, He L, Ghafoori E, Zhao X. Torsional strengthening of steel circular hollow sections (CHS) using CFRP composites. Eng Struct 2018;171:806–16.
[22] Hu L, Feng P, Zhao XL. Fatigue design of CFRP strengthened steel members. Thin-Walled Struct 2017;119(January):482–98.
[23] Kadhim MMA, Wu Z, Cunningham LS. Loading rate effects on CFRP strengthened steel square hollow sections under lateral impact. Eng Struct 2018;xxxx.
[24] Alam MI, Fawzia S, Zhao XL, Remennikov AM, Bambach MR, Elchalakani M. Performance and dynamic behaviour of FRP strengthened CFST members subjected to lateral impact. Eng Struct 2017;147:160–76.
[25] Kabir MH, Fawzia S, Chan THT, Badawi M. Durability of CFRP strengthened steel circular hollow section member exposed to sea water. Constr Build Mater 2016; 118:216–25.
[26] Seica MV, Packer JA. FRP materials for the rehabilitation of tubular steel structures, for underwater applications. Compos Struct 2007;80(3):440–50.
[27] SF. THTC. Kabir JCPHG, MH and Received. Comparative durability study of CFRP strengthened tubular steel members under cold weather. Mater Struct 10;2015.
[28] Kabir MH, Fawzia S, Chan THT, Badawi M. Numerical studies on CFRP strengthened steel circular members under marine environment. Mater Struct Constr 2016;49(10):4201–16.
[29] Kabir MH, Fawzia S, Chan THT. Durability of CFRP strengthened circular hollow steel members under cold weather: experimental and numerical investigation. Constr Build Mater 2016;123:372–83.
[30] Kabir MH, Fawzia S, Chan THT, Gamage JCPH. Durability performance of carbon fibre-reinforced polymer strengthened circular hollow steel members under cold weather. Aust J Struct Eng 2014;15(4):377–92.
[31] Keykha AH. Assessment of structural behavior of vertical curved hollow steel beams strengthened using CFRP composite. Pract Period Struct Des Constr 2019;24 (2009):1–8.
[32] ASTM A 370-19ei. Standard testing methods and definitions for mechanical testing of steel products. West Conshohocken; 2019.
[33] A. D3039/D3039M-17. Standard test methods for tensile properties of polymer matrix composite materials; 2017.
[34] Baldan A. Adhesively-bonded joints and repairs in metallic alloys, polymers and composite materials: adhesives, adhesion theories and surface pretreatment. J Mater Sci 2004;39(1):1–49.
[35] Fernando D, Yu T, Teng JG, Zhao XL. CFRP strengthening of rectangular steel tubes subjected to end bearing loads: effect of adhesive properties. Proc. 4th Int. Conf. FRP Compos. Civ. Eng. CICE 2008, no. Schnerch 2005; 2008. p. 22–24.
[36] Mahmoud K, El-Salakawy E. Behavior of full-scale railway turnout sleepers from glue-laminated fiber composite sandwich structures. J Compos Constr 2012;16 (December):724–36.
[37] El Damatty AA, Abushagur M, Youssef MA. Experimental and analytical investigation of steel beams rehabilitated using GFRP sheets. Steel Compos Struct 2003;3(6):421–38.
[38] Sika adhesive group. Product data sheet(Sika-31); 2009.
[39] Mamalis AG, Manolakos DE, Ioannidis MB, Kostazos PK. Bending of cylindrical steel tubes: numerical modelling. Int J Crashworthiness 2006;11(1):37–47.
[40] Rathnaweera G, Durandet Y, Ruan D, Hajj M. Performance of advanced high strength steel and aluminium alloy tubes in three-point bending. Sustain Automot Technol 2012, 2012,;61(03):25–32.
[41] Xia JG, Teng SH. Behaviour of FRP-to-steel bonded joints. In: Proceedings, International symposium on bond behaviour of FRP in structures; 2005.
[42] Brown D. Design of curved steel. Steel Constr Inst 2007.
[43] Ibrahim AM. The ovalisation of steel circular hollow sections under bending. 2018; 11(1):12–19.
[44] Karnovsky IA. Theory of arched structures: strength, stability, vibration, vol. 9781461404699; 2012.
[45] Elchalakani M, Zhao XL, Grzebieta R. Cyclic bending tests to determine fully ductile section slenderness limits for cold-formed circular hollow sections. J Struct Eng 2004;130(7):1001–10.